MNRAS **472,** 2643–2650 (2017)
Advance Access publication 2017 August 16
doi:10.1093/mnras/stx2104

Large-scale fluctuations in the cosmic ionizing background: the impact of beamed source emission

Teresita Suarez★ and Andrew Pontzen★
Department of Physics and Astronomy, University College London, London WC1E 6BT, UK

Accepted 2017 August 10. Received 2017 July 26; in original form 2017 June 8

ABSTRACT

When modelling the ionization of gas in the intergalactic medium after reionization, it is standard practice to assume a uniform radiation background. This assumption is not always appropriate; models with radiative transfer show that large-scale ionization rate fluctuations can have an observable impact on statistics of the Lyman α forest. We extend such calculations to include beaming of sources, which has previously been neglected but which is expected to be important if quasars dominate the ionizing photon budget. Beaming has two effects: first, the physical number density of ionizing sources is enhanced relative to that directly observed; and secondly, the radiative transfer itself is altered. We calculate both effects in a hard-edged beaming model where each source has a random orientation, using an equilibrium Boltzmann hierarchy in terms of spherical harmonics. By studying the statistical properties of the resulting ionization rate and H I density fields at redshift $z \sim 2.3$, we find that the two effects partially cancel each other; combined, they constitute a maximum 5 per cent correction to the power spectrum $P_{\mathrm{H\,I}}(k)$ at $k = 0.04\,h\,\mathrm{Mpc}^{-1}$. On very large scales ($k < 0.01\,h\,\mathrm{Mpc}^{-1}$) the source density renormalization dominates; it can reduce, by an order of magnitude, the contribution of ionizing shot noise to the intergalactic H I power spectrum. The effects of beaming should be considered when interpreting future observational data sets.

Key words: radiative transfer – diffuse radiation – large-scale structure of Universe – cosmology: theory.

1 INTRODUCTION

Intergalactic neutral hydrogen can be detected in the spectra of background quasars; absorption at the rest-frame Lyman α transition gives rise to a ‘forest’ with hundreds of distinct absorption lines corresponding to neutral hydrogen at different redshifts (Weymann, Carswell & Smith 1981). On small scales, between 1 and 40 h^{-1} Mpc comoving, the forest can be used as a statistical tracer of the distribution of matter (Viel et al. 2005).

In fact hydrogen in the intergalactic medium (IGM) at $z < 5$ is highly ionized by ultraviolet (UV) background radiation produced by stars and quasars (Croft 2004; Viel et al. 2005), leaving only a trace of H I. This UV background is therefore an essential element in simulations of the forest (Cen et al. 1994). When modelling Lyman α absorption, the neutral hydrogen density is assumed to be in ionization equilibrium with a uniform ionizing background (e.g. Katz, Weinberg & Hernquist 1996; Haehnelt et al. 2001; McDonald 2003; Croft 2004). Theoretical and observational arguments both show that this assumption can fail in various limits and a fluctuating UV background ought at least in principle to be included in analyses of the forest (Maselli & Ferrara 2005).

Recently, some attention has been devoted to understanding H I fluctuations on scales approaching the mean-free-path of an ionizing photon (Gontcho A Gontcho, Miralda-Escudé & Busca 2014; Pontzen 2014; Pontzen et al. 2014; Bautista et al. 2017). In this large-scale limit, the correlation of H I with cosmological density progressively weakens and eventually reverses sign because the clustering of the radiation field becomes stronger than the clustering of intergalactic hydrogen. Additionally, if quasars contribute significantly to the photon production budget, an uncorrelated shot-noise component is added to the power due to their intrinsic rarity.

A number of factors have been neglected from radiative transfer calculations to date, however. These include beaming of sources, variable heating from high-frequency photons and time dependence. In this paper, we tackle the first of these simplifications and explore the effect of quasar beaming on the shot-noise contribution to the large-scale diffuse H I power spectrum. We estimate the correction to the radiation fluctuations when emission is not isotropic but beamed for a random distribution of quasars.

The plan for the remainder of this paper is as follows. In Section 2, we derive the emissivity power spectrum accounting

★ E-mail: teresita.noguez.13@ucl.ac.uk (TS); a.pontzen@ucl.ac.uk (AP)

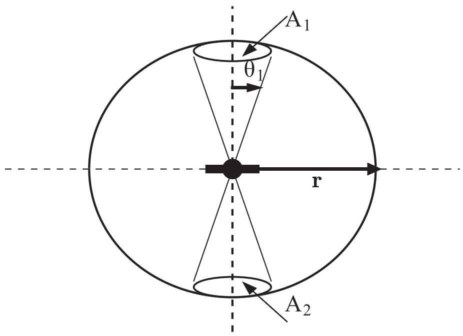

Figure 1. Geometry of our source model, which represents a quasar with variable beam width. The probability of detecting a quasar is proportional to the beam area A_1 and A_2. These in turn are determined by the opening angle, here parametrized by θ_1 with $0 < \theta_1 \leq \pi/2$. The isotropic case is recovered when $\theta_1 = \pi/2$.

for a population of sources with fixed beam widths but random orientations. In Section 3, we discuss the radiation transfer equation appropriate for this distribution (with further detail in the Appendix). We present the resulting power spectrum of the radiation and H I fluctuations in Section 4 and summarize in Section 5.

2 FLUCTUATIONS IN THE EMISSIVITY

2.1 Correcting the number density of sources $\bar{n}$

The simplest effect of source beaming is that the underlying number density $\bar{n}$ is no longer directly measured by observations. The observed number density $\bar{n}_{\rm obs}$ must be corrected for the probability of being detected. This probability is given by the area of the emission (the beam) divided by the total area of a sphere, assuming a random orientation. We assume a hard-edged beam with opening angle $2\theta_1$; see Fig. 1. The chance of any given quasar to be seen is then

$$p(\text{seen}) = \frac{(A_1 + A_2)}{4\pi r^2} = 1 - \cos\theta_1, \tag{1}$$

in which A_1 and A_2 are the areas of two axisymmetric beams. The isotropic case is recovered when the angle θ_1 is equal to $\pi/2$. In the limit that θ_1 approaches zero, the emission becomes a pencil-beam and the likelihood of observation becomes extremely small.

The number of density sources we detect, $\bar{n}_{\rm obs}$, is the true mean density $\bar{n}$ times the probability for observing each one:

$$\bar{n}_{\rm obs} = \bar{n}(1 - \cos\theta_1). \tag{2}$$

In Pontzen (2014; henceforth P14), it was assumed that these two densities are equal; for the results in this work, we fix $\bar{n}_{\rm obs}$ at the value estimated by P14, meaning that the underlying density $\bar{n}$ varies. We emphasize that $\bar{n}_{\rm obs}$ is itself highly uncertain, but that for the purpose of understanding the effects of beaming it is simplest to keep it fixed.

2.2 Definitions required for the emissivity derivation

In the remainder of Section 2, we will calculate the effects of beaming on the emissivity power spectrum from discrete sources. A fraction of photons comes from recombination of the IGM, but following the approach of P14 we account for those through an appropriate additional term in the radiative transfer equation (see Section 3). Here, we can therefore focus on the discrete sources alone.

We start from a rate of emission of photons in a narrow band at frequency ν, in a small volume around comoving position $\boldsymbol{x}$ and in an interval around the direction vector $\boldsymbol{n}$; this is denoted $j_\nu(\boldsymbol{x}, \boldsymbol{n})$. As in P14, we simplify to a frequency-averaged quantity $j(\boldsymbol{x}, \boldsymbol{n})$ where

$$j(\boldsymbol{x}, \boldsymbol{n}) = \int j_\nu(\boldsymbol{x}, \boldsymbol{n})\sigma_{\rm H\,I}(\nu)\mathrm{d}\nu. \tag{3}$$

The goal is to model fractional variations of j around its mean value $\langle j \rangle$, motivating the definition

$$\delta_j(\boldsymbol{x}, \boldsymbol{n}) = \frac{j(\boldsymbol{x}, \boldsymbol{n})}{\langle j \rangle} - 1. \tag{4}$$

We assume that variations on sufficiently large scales can be related to the cosmological matter overdensity δ_ρ multiplied by a constant bias b_j, plus a Gaussian white-noise field to represent shot noise from the the rarity of sources. The variations of the emissivity, δ_j, on large scales is therefore written:

$$\delta_j(\boldsymbol{x}, \boldsymbol{n}) = b_j\delta_\rho(\boldsymbol{x}) + \delta_{j,\rm SN}(\boldsymbol{x}, \boldsymbol{n}), \tag{5}$$

where δ_ρ is the fractional matter overdensity at position $\boldsymbol{x}$. According to equation (5), we need only to consider the component $\delta_{j,\,\rm SN}$ in the present work; by construction all angle-dependence arises in the shot-noise term and the radiation fluctuations that correlate with the cosmological density field will not be altered by beaming. As a final simplification, P14 section II.C argues that the shot-noise contribution from galaxies is negligible (owing to their very high number density) and we can assume all contributions to $\delta_{j,\,\rm SN}$ arise from quasars.

In the remainder of this paper, we will often need to work with Fourier-transformed and spherical harmonic representations of functions. For any function $F(\boldsymbol{x}, \boldsymbol{n})$, these are defined, respectively, as

$$\tilde{F}(\boldsymbol{k}, \boldsymbol{n}) \equiv \frac{1}{(2\pi)^{3/2}} \int \mathrm{d}^3\boldsymbol{x}\; e^{-i\boldsymbol{k}\cdot\boldsymbol{x}}\; F(\boldsymbol{x}, \boldsymbol{n}) \text{ and} \tag{6}$$

$$F^{\ell m}(\boldsymbol{x}) \equiv \int \mathrm{d}^2\boldsymbol{n}\; Y^*_{\ell m}(\boldsymbol{n})F(\boldsymbol{x}, \boldsymbol{n}), \tag{7}$$

where $Y^*_{\ell m}(\boldsymbol{n})$ is the complex conjugate spherical harmonic basis function as defined in Varshalovich, Moskalev & Khersonskii (1988). The spherical harmonic Fourier modes $\tilde{F}^{\ell m}(\boldsymbol{k})$ follow by Fourier-transforming equation (7) or, equivalently, taking spherical harmonics of equation (6).

2.3 Emission of one quasar with a preferred alignment

We want to understand the statistical properties of the $\boldsymbol{j}(x, n)$ field accounting for anisotropic emission from the sources. To start, consider a single quasar of luminosity L inside a fixed volume V. Adopting at first an aligned coordinate system such that θ gives the angle to the symmetry axis, and using the geometry of Section 2.1, we have

$$j_{\rm aligned}(\theta, \phi) = J \begin{cases} 1 & 0 < \theta < \theta_1 \\ 0 & \theta_1 < \theta < \pi - \theta_1 \\ 1 & \pi - \theta_1 < \theta < \pi \end{cases}, \tag{8}$$

where $j_{\rm aligned}(\theta, \phi)$ indicates the emissivity for the single quasar in our preferred coordinate system, the constant J is defined by $J = L/(4\pi V(1 - \cos\theta_1))$, and θ_1 is the angle described in Section 2.1 and can have any value in the interval $[0, \pi/2]$.

To proceed further, we decompose the function $j_{\rm aligned}(\theta,\ \phi)$ into spherical harmonics $j^{\ell m}_{\rm aligned}$ according to equation (7). For our aligned choice of coordinates, we only need to consider $m = 0$ terms because of the cylindrical symmetry around the $\hat{z}$-axis. In this case, the spherical harmonic $Y_{\ell 0}(\theta, \phi)$ can be written in terms of a Legendre polynomial, $Y_{\ell 0}(\theta, \phi) = \sqrt{(2l+1)/(4\pi)} P_\ell(\cos\theta)$. Using this result and the recursion relations for P_ℓ, we can express the emissivity variations as

$$J_\ell \equiv j^{\ell 0}_{\rm aligned} = J \begin{cases} \sqrt{4\pi}(1-\cos\theta_1) & \ell = 0; \\ \sqrt{\frac{\pi}{2\ell+1}} \left[1-(-1)^{\ell+1}\right] \left[P_{\ell-1} - P_{\ell+1}\right] & \ell > 0, \end{cases} \tag{9}$$

where for brevity we have written the Legendre polynomials evaluated at $\cos\theta_1$, i.e. $P_{l-1} \equiv P_{l-1}(\cos\theta_1)$ and $P_{l+1} \equiv P_{l+1}(\cos\theta_1)$.

2.4 Emission of *N* quasars with no preferred alignment

So far we have derived the emissivity for a single quasar in a volume V in terms of the spherical harmonics coefficients. However, we now need to look at the realistic case of N quasars, each with a beam pointing in an independent random direction. To achieve this, we first need to drop the assumption of a preferred coordinate system, even for the single-quasar case $N = 1$.

The spherical harmonic coefficients $j^{\ell m}_{N=1}$ for a single quasar pointing in an arbitrary direction are related to the aligned spherical harmonics via the Wigner D matrix, which expresses a rotation by Euler angles ϕ, θ, ψ:

$$\begin{aligned} j^{\ell m}_{N=1} &= \sum_{m'} D^\ell_{mm'}(\phi,\theta,\psi)\, j^{\ell m'}_{\rm aligned} \\ &= D^\ell_{m0}(\phi,\theta,\psi)\, J_\ell. \end{aligned} \tag{10}$$

We are thus only interested in the value of the D matrix when $m' = 0$, for which case we have the identity (Varshalovich et al. 1988):

$$D^\ell_{m0}(\phi,\theta,\psi) = \sqrt{\frac{4\pi}{2\ell+1}}\, Y^*_{\ell m}(\theta,\phi). \tag{11}$$

The average emissivity over all possible beam alignment Euler angles is now given by

$$\begin{aligned} \left\langle j^{\ell m}_{N=1} \right\rangle_{\phi,\theta,\psi} &\equiv \frac{1}{8\pi^2} \iiint {\rm d}\theta {\rm d}\phi {\rm d}\psi \sin\theta\, D^\ell_{m0}(\theta,\phi,\psi)\, J_\ell \\ &= \begin{cases} J_0 & \ell = 0; \\ 0 & \ell \neq 0. \end{cases} \end{aligned} \tag{12}$$

Next, we need to calculate the two-point statistic $\langle j^{\ell m}_{N=1} j^{*\ell' m'}_{N=1} \rangle$. Still using a single quasar averaged over all possible directions we obtain

$$\left\langle j^{\ell m}_{N=1} j^{*\ell' m'}_{N=1} \right\rangle_{\phi,\theta,\psi} = \frac{1}{2\ell+1} \begin{cases} J^2_\ell\, \ell = \ell', & m = m'; \\ 0 & \text{otherwise}, \end{cases} \tag{13}$$

where we used the orthogonality properties of the spherical harmonics.

If N sources contribute, the angle-averaged emissivity (12) is simply scaled up by a factor N. However, the generalization of the two-point function requires a more careful analysis. The total emissivity $j^{\ell m}_N$ in this case can be decomposed as the sum of emissivity due to the individual sources,

$$j^{\ell m}_N = \sum_{i=1}^{N} j^{\ell m}_{(i)}, \tag{14}$$

where $j^{\ell m}_{(i)}$ represents the emission due to the ith source. When taking an average over all possible orientations, each now has its own Euler angles ϕ_i, θ_i, ψ_i. Considering the two-point function,

$$\left\langle j^{\ell m}_N j^{*\ell' m'}_N \right\rangle_{\{\phi_i,\theta_i,\psi_i\}} = \sum_{a=1}^{N} \sum_{b=1}^{N} \left\langle j^{\ell m}_{(a)} j^{\ell' m'}_{(b)} \right\rangle_{\{\phi_i,\theta_i,\psi_i\}}, \tag{15}$$

there are now two types of term. First, there are the single-source terms where $a = b$. In these cases, the average over Euler angles is no different from the $N = 1$ case. Since there are N such terms with $a = b$, they contribute N times the result in equation (13). Secondly, there are cross-quasar terms where $a \neq b$. These terms involve separately integrating over the Euler angles for both a and b. The decoupled integrals are individually of the form (12); each cross-term (of which there are $N^2 - N$ in total) therefore contributes J_0^2 when $\ell = 0$ and zero otherwise. Putting together the results above we find that

$$\left\langle j^{\ell m}_N j^{*\ell' m'}_N \right\rangle_{\{\phi_i,\theta_i,\psi_i\}} = \frac{1}{2\ell+1} \begin{cases} N^2 J_0^2 & \ell = \ell' = m = m' = 0; \\ N J_\ell^2 & \ell = \ell' \neq 0, m = m'; \\ 0 & \text{otherwise}. \end{cases} \tag{16}$$

This is the final result for the case of a fixed number of N quasars inside a volume V.

2.5 Putting it together: emissivity shot-noise power spectrum

So far we have considered a case where the emissivity inside a fixed volume V with a known number of quasars N is calculated. We now need to introduce fluctuations in N. We expect to have $\langle N \rangle = \bar{n} V$ quasars, where the average is over all possible values of N and $\bar{n}$ is the number density. In the Gaussian limit of Poisson statistics (which should be appropriate on large scales), we also know that the variance in N is given by the relation $\langle N^2 \rangle - \langle N \rangle^2 = \bar{n} V$. Consequently, the statistics for the emissivity j_V in a fixed volume but with varying N are specified by

$$\begin{aligned} &\left\langle j^{\ell m}_V j^{*\ell' m'}_V \right\rangle \\ &= \frac{1}{2\ell+1} \begin{cases} \left[\bar{n} V + (\bar{n} V)^2\right] J_0^2 & \ell = \ell' = m = m' = 0; \\ \bar{n} V J_\ell^2 & \ell = \ell' \neq 0, m = m'; \\ 0 & \text{otherwise}, \end{cases} \end{aligned} \tag{17}$$

where the average is now over all values of N, as well as over the Euler angles ϕ_i, θ_i, ψ_i for each quasar.

To make the connection with the statistics of the $\delta_{j,\rm SN}$ field introduced in equation (5), we now define the fractional variations in j in a volume V as $\delta_{j,V}$ where

$$\delta_{j,V}(\boldsymbol{n}) \equiv \frac{j_V(\boldsymbol{n}) - \langle j_V \rangle}{\langle j_V \rangle}, \tag{18}$$

which implies the spherical harmonic expansion is given by

$$\delta^{\ell m}_{j,V} = \frac{j^{\ell m}_V - \langle j^{\ell m}_V \rangle}{\langle j^{00}_V \rangle} \sqrt{4\pi}. \tag{19}$$

Using this result alongside equation (17), we find that $\langle \delta^{\ell m}_{j,V} \rangle = 0$ and

$$\left\langle \delta^{\ell m}_{j,V} \delta^{*\ell' m'}_{j,V} \right\rangle = \frac{1}{\bar{n} V} \frac{4\pi}{2\ell+1} \begin{cases} (J_\ell / J_0)^2 & \ell = \ell', m = m'; \\ 0 & \text{otherwise}. \end{cases} \tag{20}$$

Finally, the expression for the statistics averaged over a volume V need to be related to the power spectrum of $\delta_{j,\rm SN}$. We define the source shot-noise power spectrum $P_{j,{\rm SN},\ell}(\boldsymbol{k})$ via

$$\left\langle \tilde{\delta}^{\ell m}_{j,\rm SN}(\boldsymbol{k}) \tilde{\delta}^{*\ell' m'}_{j,\rm SN}(\boldsymbol{k}') \right\rangle = P_{j,{\rm SN},\ell}(\boldsymbol{k}) \delta_{\rm D}(\boldsymbol{k} - \boldsymbol{k}') \delta_{\ell\ell'} \delta_{mm'}, \tag{21}$$

where $\delta_{\rm D}$ is the Dirac delta function. To make contact between this required form and the derivation so far, one calculates the fluctuation averaged over a volume V:

$$\delta^{\ell m}_{j,V} \equiv \frac{1}{V}\int_V \mathrm{d}^3x\ \delta^{\ell,m}_{j,\rm SN}(\boldsymbol{x}) = \frac{1}{(2\pi)^{3/2}V}\int_V \mathrm{d}^3x \int \mathrm{d}^3k\ e^{i\boldsymbol{k}\cdot\boldsymbol{x}}\tilde{\delta}^{\ell,m}_{j,\rm SN}(\boldsymbol{k}). \quad (22)$$

Making the ansatz that $P_{j,{\rm SN},\ell}(k)$ is in fact independent of k (as expected for shot noise), we find that

$$\left\langle \delta^{\ell m}_{j,V}\delta^{*\ell' m'}_{j,V}\right\rangle = \frac{1}{V}P_{j,{\rm SN},\ell}\delta_{\ell\ell'}\delta_{mm'}. \quad (23)$$

By comparing with equation (20) one obtains the final result:

$$P_{j,{\rm SN},\ell}(k) = \frac{4\pi}{\bar{n}}\frac{(J_\ell/J_0)^2}{2\ell+1}. \quad (24)$$

In the case of isotropic emission, $J_\ell = 0$ for $\ell > 0$ and the result (24) agrees with that from P14. Note that the shot noise always scales with the inverse of the mean density $\bar{n}$ (whether or not the emission is isotropic).

3 RADIATIVE TRANSFER METHOD

In this section, we expand the P14 linearized radiative transfer equation into a spherical harmonic Boltzmann hierarchy so that we can use the directional source statistics derived in Section 2. Starting from the physical number density of photons $f(\boldsymbol{x}, \boldsymbol{n}, \nu)$ at comoving position $\boldsymbol{x}$ travelling in direction $\boldsymbol{n}$ with frequency ν, P14 integrates over the frequency dependence ν by defining

$$f_{\rm LL}(\boldsymbol{x}, \boldsymbol{n}) = \int \mathrm{d}\nu\ f(\boldsymbol{x}, \boldsymbol{n}, \nu)\sigma_{\rm H\,I}(\nu), \quad (25)$$

analogous to equation (3). We approximate the radiation and ionization to be in equilibrium; this is a good approximation at redshift $z \sim 2.3$ (e.g. Busca et al. 2013). The fractional variations around the mean value of $f_{\rm LL}$ are denoted $\delta_{f_{\rm LL}}$; by linearizing the Boltzmann equation, P14 obtained

$$\left[i(a\ \kappa_{\rm tot,0})^{-1}(\boldsymbol{n}\cdot\boldsymbol{k}) + 1\right]\tilde{\delta}_{f_{\rm LL}}(\boldsymbol{k}, \boldsymbol{n}) = (1-\beta_{\rm H\,sci}\beta_{\rm r})\tilde{\delta}_j(\boldsymbol{k}, \boldsymbol{n}) + \beta_{\rm H\,I}\beta_{\rm r}[\tilde{\delta}_{n_{\rm H\,I}} + \tilde{\delta}_\Gamma(\boldsymbol{k})] - \tilde{\delta}_{\kappa_{\rm tot}}. \quad (26)$$

Here, a is the cosmological scalefactor and $\kappa_{\rm tot}$ an effective opacity to ionizing photons (composed of both physical absorption and corrections from effects such as redshifting). The mean effective opacity is given by $\kappa_{\rm tot,0} \equiv \langle\kappa_{\rm tot}\rangle$ while its fractional fluctuations are specified by $\delta_{\kappa_{\rm tot}}$. The inverse of $a\,\kappa_{\rm tot,\,0}$ gives the effective comoving mean free path of an ionizing photon, which can be estimated to be 350 Mpc at $z = 2.3$ (see P14 equation 16). The dimensionless quantities $\beta_{\rm H\,I}$ and β_r quantify, respectively, the fraction of effective opacity resulting from physical absorption in the IGM, and the fraction of H I recombinations that result in an emission of a new ionizing photon. The appearance of β_r is in fact accounting for ionizing photons re-emitted (isotropically) from the IGM itself as mentioned at the start of Section 2.2. For full details see P14.

In the same way that equation (5) decomposes the emissivity into shot noise and cosmological terms, we can decompose the radiation density fluctuations:

$$\tilde{\delta}_{f_{\rm LL}}(\boldsymbol{k}, \boldsymbol{n}) = \tilde{\delta}_{f_{\rm LL},\rm SN}(\boldsymbol{k}, \boldsymbol{n}) + b_{f_{\rm LL}}(\hat{\boldsymbol{k}}\cdot\boldsymbol{n})\tilde{\delta}_\rho(\boldsymbol{k}), \quad (27)$$

where $b_{f_{\rm LL}}$ is a scale- and direction-dependent bias. At linear order, $\tilde{\delta}_{f_{\rm LL},\rm SN}$ depends only on $\tilde{\delta}_{j,\rm SN}$, not on the cosmological density $\tilde{\delta}_\rho$. In the present analysis, we revise only the shot-noise component.

P14 assumes that $\delta_{j,\,\rm SN}$ is independent of $\boldsymbol{n}$. In our case, we can no longer make this assumption. Instead we write the direction vector $\boldsymbol{n} = (\sin\theta\cos\phi, \sin\theta\sin\phi, \cos\theta)$ and, to simplify the analysis, rotate the coordinate system[1] such that the wavevector $\boldsymbol{k}$ lies along the $\hat{z}$-axis, i.e. $\boldsymbol{k} = (0, 0, k)$. The product $\boldsymbol{n}\cdot\boldsymbol{k}$ appearing in the radiative transfer equation then expands to

$$\boldsymbol{n}\cdot\boldsymbol{k} = k\ \cos\theta = \sqrt{\frac{4\pi}{3}}\ k\ Y_{10}(\theta, \phi). \quad (28)$$

Using this result in equation (26), we obtain (see the Appendix for a detailed derivation):

$$\tilde{\delta}^{\ell m}_{f_{\rm LL},\rm SN} - \beta_{\rm H\,I}\delta^{00}_{f_{\rm LL},\rm SN}\delta_{0\ell}\delta_{0m} + \frac{ik}{a\ \kappa_{\rm tot,0}} \times \left\{\tilde{\delta}^{\ell-1,m}_{f_{\rm LL},\rm SN}\sqrt{\frac{(\ell+m)(\ell-m)}{(2\ell-1)(2\ell+1)}} + \tilde{\delta}^{\ell+1,m}_{f_{\rm LL},\rm SN}\sqrt{\frac{(\ell+m+1)(\ell-m+1)}{(2\ell+1)(2\ell+3)}}\right\} = (1-\beta_{\rm H\,I}\beta_{\rm r})\tilde{\delta}^{\ell m}_{j,\rm SN}(\boldsymbol{k}), \quad (29)$$

where the explicit $\boldsymbol{k}$-dependence of $\tilde{\delta}^{\ell m}_{f_{\rm LL}}$ has been omitted from the expression for brevity. The expression can be rewritten schematically as

$$\sum_{\ell'}\mathbf{M}_{m\ell\ell'}(\boldsymbol{k})\delta^{\ell' m}_{f_{LL},\rm SN}(\boldsymbol{k}) = (1-\beta_{\rm H\,I}\beta_r)\delta^{\ell m}_{j,\rm SN}(\boldsymbol{k}), \quad (30)$$

where $\mathbf{M}_{m\ell\ell'}(\boldsymbol{k})$ contains the appropriate equilibrium radiation transfer coefficients from the left-hand side of (29). We can invert the linear relationship:

$$\tilde{\delta}^{\ell m}_{f_{\rm LL},\rm SN}(\boldsymbol{k}) = (1-\beta_{\rm H\,I}\beta_{\rm r})\sum_{\ell'}\mathbf{M}^{-1}_{m\ell\ell'}(\boldsymbol{k})\tilde{\delta}^{\ell' m}_{j,\rm SN}(\boldsymbol{k}), \quad (31)$$

where the inverse matrix $\mathbf{M}^{-1}_m$ satisfies

$$\sum_{\ell'}\mathbf{M}^{-1}_{m\ell\ell'}\mathbf{M}_{m\ell'\ell''} = \delta_{\ell\ell''}. \quad (32)$$

In our analysis, we are only interested in the overall radiation intensity fluctuations – i.e. the statistical properties of $\tilde{\delta}^{00}_{f_{\rm LL}}$, or equivalently $\tilde{\delta}_\Gamma$. Therefore, we need to consider only the $m = 0$ component of equation (31) since different ms do not couple to each other.

The next step is to solve the inversion (31) numerically. For these purposes, the hierarchy must be truncated at finite $\ell_{\rm max}$, so that we solve a $\ell_{\rm max}\times\ell_{\rm max}$ matrix inversion for each k. In practice, choosing $\ell_{\rm max}$ requires a convergence test to ensure that any results are insensitive to the finite truncation.

In the case of an isotropically radiating source, the solution for $\tilde{\delta}_\Gamma$ was written in closed form by equation (30) of P14, which can be rearranged (see the Appendix) to provide a test case that is illustrated in Fig. 2. Specializing our equation (31) to the isotropic case corresponds to setting $\tilde{\delta}^{\ell m}_j$ to zero for $\ell \neq 0$ and $m \neq 0$. The result for $\delta_\Gamma = \delta^{00}_{f_{\rm LL}}/\sqrt{4\pi}$ is shown in Fig. 2 as a function of $k/(a\,\kappa_{\rm tot,\,0})$.

[1] This freedom is available because we will ultimately consider only scalar quantities such as the ionization rate and H I density. Statistical isotropy will then ensure the choice of $\hat{\boldsymbol{k}}$ direction in the analysis is irrelevant. Note that our special coordinate system in this section is independent of the alternative preferred system temporarily adopted in the early parts of Section 2.

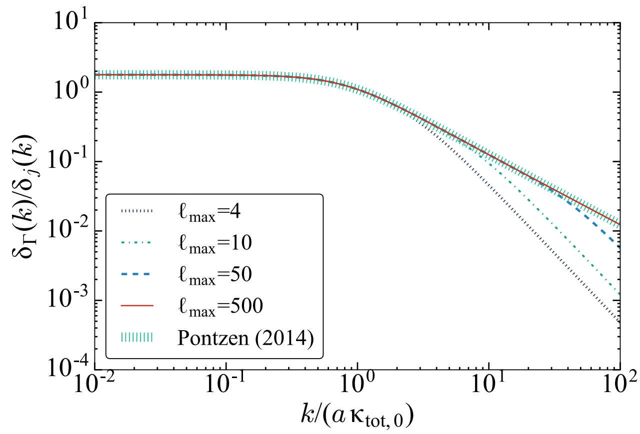

Figure 2. Demonstration of convergence of the numerical solution for shot noise-induced ionization rate fluctuations $\tilde{\delta}_{\Gamma,\mathrm{SN}}(\boldsymbol{k})$ as a fraction of the underlying source fluctuations $\tilde{\delta}_{j,\mathrm{SN}}(\boldsymbol{k})$. We choose an isotropic emission case where a closed-form analytic solution (shown by the shading) is known from Pontzen (2014). As $\ell_{\max}$ increases for test values from 4 to 500, our numerical hierarchy converges to this solution.

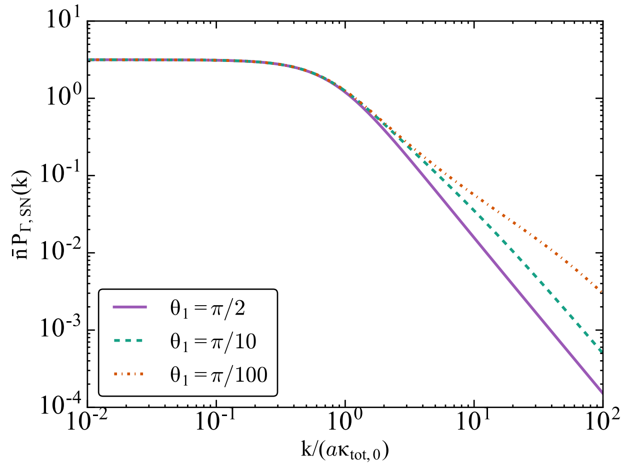

Figure 3. Shot-noise power spectrum for radiation fluctuations $P_{\Gamma,\mathrm{SN}}(k)$, multiplied by the overall density of sources $\bar{n}$ (which removes the only dependence on $\bar{n}$). For the solid, dashed, and dash–dotted lines the opening angle for the radiation sources is $\pi/2$, $\pi/10$ and $\pi/100$, respectively. The low-k radiation fluctuations are independent of the beam angle while at high k the amplitude of fluctuations are increased for narrow beams.

Consider first the closed-form solution from P14, shown by the shaded band. The function shows how ionization rate fluctuations trace emissivity fluctuations on large scales (small k) – the function converges to a fixed, order unity value. On small scales (large k), the fluctuations in the ionization rate are suppressed: even a point source of radiation can ionize extended regions of space, so the small-scale ionization rate fluctuations are damped. The transition scale between these behaviours is set by the effective mean free path $(a\,\kappa_{\mathrm{tot},\,0})^{-1}$.

As $\ell_{\max}$ increases, our new hierarchy solution correctly converges to the closed-form solution (dotted, dash–dotted, dashed and solid lines, respectively, for $\ell_{\max} = 4$, 10, 50 and 500). The long wavelength limit (small k), is completely insensitive to $\ell_{\max}$, while the highest k modes are most sensitive. Note that while in this test case the emission is isotropic, the actual radiation field is not; there is a net flux of photons away from the plane wave peaks which defines a preferred direction. This accounts for the sensitivity to $\ell_{\max}$; as k becomes large the spacing between peaks becomes small compared to the mean free path of a photon. The true photon distribution is sharply peaked in the $\hat{\boldsymbol{k}}$ direction and such sharp directionality requires a high $\ell_{\max}$ for an adequate representation. In the remainder of this paper, we set $\ell_{\max} = 500$; we verified that increasing $\ell_{\max}$ to 1000 did not change our results.

4 RESULTS FOR IONIZATION RATE AND H I POWER SPECTRA

We now have everything required to consider the power spectrum of radiation fluctuations for different source beaming parameters. Again considering only the shot-noise component, we can write

$$P_{\Gamma,\mathrm{SN}}(k) = \frac{(1-\beta_{\mathrm{H\,I}}\beta_r)^2}{4\pi}\sum_{\ell}(\mathbf{M}^{-1}_{00\ell}(k))^2 P_{j,\mathrm{SN},\ell}(k), \tag{33}$$

where $P_{j,\,\mathrm{SN},\,\ell}(k)$ is given by equation (24) and is in fact independent of k. The term $\mathbf{M}^{-1}_{00\ell}(k)$ refers to the inverse matrix $\mathbf{M}^{-1}_{m\ell'\ell}$ in equation (32) with $m = 0$ and $\ell' = 0$; in general there is no closed analytic form so, as described in Section 3, the matrix must be inverted numerically.

Fig. 3 plots $\bar{n}\,P_{\Gamma,SN}(k)$ against the wavenumber for different values of the beam width $\theta_1 = \pi/2$, $\pi/10$ and $\pi/100$. These correspond to opening angles of 180°, 36° and 3°.6, respectively; the last of these is exceptionally narrow compared to observational estimates of $\gtrsim$30° (Trainor & Steidel 2013) and should be regarded as an extreme upper limit on the magnitude of the correction.

Because $P_{j,\mathrm{SN},\ell}(k)$ scales inversely proportional to the source density $\bar{n}$, the product $\bar{n}\,P_{\Gamma,\mathrm{SN}}(k)$ is independent of $\bar{n}$ and a function only of the beam shape. Inspecting this product allows us to isolate and understand the effect of the beaming.

The first case, $\theta_1 = \pi/2$, is plotted with a solid line and recovers the isotropic-emission solution (as previously illustrated in Fig. 2). As θ_1 decreases (dashed and dash-dotted lines, respectively), the radiation emission is increasingly tightly collimated. The effect of the beaming on $\bar{n}\,P_{\Gamma,\mathrm{SN}}(k)$ is, however, confined to large k. At low k, where the mean-free path $(a\kappa_{\mathrm{tot}})^{-1}$ is small compared to the wave under consideration, beaming has no effect because the local ionizing rate scales proportionally to the total photon output of sources. For smaller wavelengths (higher k), narrow beams lead to higher amplitude fluctuations in the ionizing photon field.

Until now, we have considered only the shot-noise contribution, but to draw overall conclusions we need to put our revised radiation shot noise estimates back into the full calculation from P14. Because the shot noise is uncorrelated with the cosmological fluctuations in the first-order analysis, the power spectra add linearly:

$$\mathrm{P}_{\mathrm{H\,I}}(k) = b^2_{\mathrm{H\,I}}(k)\mathrm{P}_\rho(k) + \mathrm{P}_{\mathrm{H\,I,SN}}(k), \tag{34}$$

where $P_\rho(k)$ is the dark matter density power spectrum and $b_{\mathrm{H\,I}}$ is the linear relationship between H I density and the total density as a function of scale, which is unchanged from P14. Finally, because $\delta_{n_{\mathrm{H\,I}},\mathrm{SN}} = -\delta_{\Gamma,\mathrm{SN}}$, the shot-noise power spectra for H I and Γ are equal and we have

$$\mathrm{P}_{\mathrm{H\,I}}(k) = b^2_{\mathrm{H\,I}}\mathrm{P}_\rho(k) + \mathrm{P}_{\Gamma,\mathrm{SN}}(k), \tag{35}$$

which allows us to use the result obtained in equation (33) for our beamed shot-noise estimates.

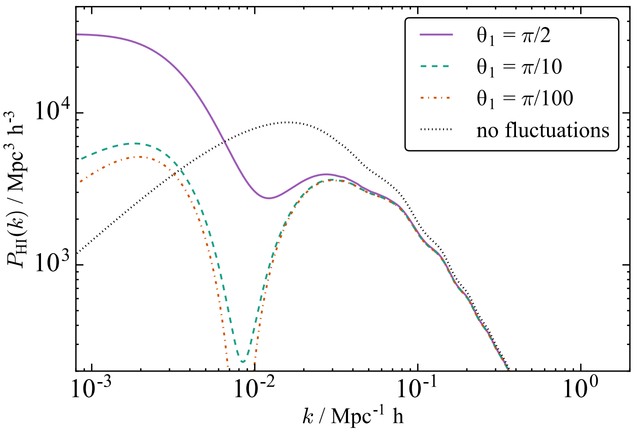

Figure 4. Power spectrum of the H I fluctuations defined by equation (35), evaluated at redshift $z \simeq 2.3$ for a fixed observed source density of $\bar{n}_{\rm obs} = 10^{-4}\ h^3\ {\rm Mpc}^{-3}$, and for the same range of beam widths θ_1 adopted in Fig. 3. All other parameters are set to the defaults from Pontzen (2014). The dominant effect of changing θ_1 arises from the rescaling of $\bar{n}$ to match $\bar{n}_{\rm obs}$; this can be seen on the largest scales (small k) where shot-noise effects dominate. The dotted line shows, for reference, the H I power spectrum in the unphysical limit where there are no UV fluctuations.

Fig. 4 shows the total power spectrum for the three values of θ_1 previously adopted and a fixed density of observed sources $\bar{n}_{\rm obs} = 1 \times 10^{-4}\ h^3\ {\rm Mpc}^{-3}$, a value adopted directly from P14. Note that for our present investigation, we assume that all sources have the same opening angle (in particular ignoring the distinction between quasars and galaxies in this respect). Even if galaxies contribute comparable or larger number of photons to the overall background, the shot noise is still strongly dominated by quasars (P14) and so this approximation is likely valid.

As in P14, radiation can be approximated as near-uniform for the power spectrum on scales below the mean-free path (for $k \gg 0.01\,h\,{\rm Mpc}^{-1}$); consequently the corrections from the fluctuating ionization always increase towards large scales. On very large scales ($k < 0.01\,h\,{\rm Mpc}^{-1}$), radiation fluctuations actually dominate over H density fluctuations in the HI power spectrum. At the transition scale, there is a characteristic dip where the radiation and H density fluctuations approximately cancel. These basic features are preserved when beaming is included.

As the source beams narrow, the results in Fig. 4 show that the primary effect is to reduce the amplitude of shot-noise fluctuations in the very large-scale regime ($k \ll 0.01\,h\,{\rm Mpc}^{-1}$) through the renormalization discussed in Section 2.1. Unlike the direct effect of the beam, this observational correction to the inferred number densities applies equally over all scales, making it extremely significant in the low-k regime where shot noise dominates. However, note that the constraining effect of current and future surveys is quite poor on such extreme scales (Pontzen et al. 2014; Bautista et al. 2017). At scales $k \sim 0.04\,h\,{\rm Mpc}^{-1}$, where reasonable observational precision can be expected in future pipelines, the effects of beaming are considerably more modest constituting a $\lesssim 5$ per cent correction. In this regime, the decreased power from the source density renormalization is partially cancelled by the increased power from the beaming itself (Fig. 3).

Because the effects are so strongly scale-dependent, and survey sensitivities are also a steep function of scale, the observability of beaming will be strongly dependent on details of observing strategy and pipelines.

5 SUMMARY AND DISCUSSION

We have constructed a model to treat fluctuations in the cosmological UV background taking into account, for the first time, anisotropy due to phenomena such as quasar beaming. To do that, we built upon the monochromatic, equilibrium, large-scale description presented in Pontzen (2014) but included angle-dependent emission terms.

We first introduced a correction for the observational bias that individual quasars are less likely to be detected if they are tightly beamed. This renormalizes the underlying density of quasars in the Universe. We then derived the emissivity shot-noise power spectrum corresponding to a distribution of quasars each pointing in a randomized direction. This required adopting an underlying beaming model; for simplicity we used a hard-edged beam of fixed opening angle $2\theta_1$ for the entire population (Fig. 1). Finally, we rederived the radiative transfer for the shot noise taking into account the new angle-dependence. These results are most naturally expressed in terms of a hierarchy of spherical harmonic coefficients; because we are only interested in the overall radiation intensity fluctuations we ultimately took the $\ell = 0$, $m = 0$ component.

We solved the new hierarchy numerically and showed that, for sufficiently large $\ell_{\rm max}$, the method converges to the known isotropic-emission case when $\theta_1 = \pi/2$ (see Fig. 2) demonstrating the accuracy of the method. Then, we explored the effects of the quasar beam width on the shot noise (Fig. 3).

The shot-noise power spectrum of radiation fluctuations $P_{\Gamma,\,\rm SN}$ in Fig. 3 shows that the fluctuations are not sensitive to the beam angle at low k. Fluctuation amplitudes do increase at high k for narrower beams; however the effect is modest even for extreme values of the beam width θ_1.

When combining the new shot-noise solution with the cosmological density fluctuations (Fig. 4), we found that the primary effect of beaming is in fact the first and simplest one: the observational renormalization of the underlying density of bright sources. This affects all k modes equally (scaling up and down the overall contribution of shot noise) and therefore is highly significant on large scales (small k) where the shot-noise potentially dominates over the cosmological signal.

This paper has focused on clarifying one area where the effects of radiative transfer on the Lyman α forest were not known. If future pipelines lead to constraints on the magnitude of this effect (e.g. Pontzen et al. 2014; Bautista et al. 2017), there are a number of other possible influences that still require to be understood. For example, time variability of sources and the effects of patchy heating still need to be incorporated in a coherent framework and will be tackled in future work.

ACKNOWLEDGEMENTS

TS acknowledges support via studentships from CONACyT (Mexico) and UCL. AP is supported by the Royal Society. The authors would like to thank Hiranya Peiris for many useful discussions and helpful comments on a draft.

REFERENCES

Bautista J. E. et al., 2017, A&A, 603, p. 23
Busca N. G. et al., 2013, A&A, 552, A96
Cen R., Miralda-Escudé J., Ostriker J. P., Rauch M., 1994, ApJ, 437, L9
Croft R. A. C., 2004, ApJ, 610, 642

Gontcho A Gontcho S., Miralda-Escudé J., Busca N. G., 2014, MNRAS, 442, 187
Haehnelt M. G., Madau P., Kudritzki R., Haardt F., 2001, ApJ, 549, L151
Katz N., Weinberg D. H., Hernquist L., 1996, ApJS, 105, 19
Maselli A., Ferrara A., 2005, MNRAS, 364, 1429
McDonald P., 2003, ApJ, 585, 34
Pontzen A., 2014, Phys. Rev. D, 89, 083010
Pontzen A., Bird S., Peiris H., Verde L., 2014, ApJ, 792, L34
Trainor R., Steidel C. C., 2013, ApJ, 775, L3
Varshalovich D. A., Moskalev A. N., Khersonskii V. K., 1988, Quantum Theory of Angular Momentum. World Scientific Publishing Co.
Viel M., Lesgourgues J., Haehnelt M. G., Matarrese S., Riotto A., 2005, Phys. Rev. D, 71, 063534
Weymann R. J., Carswell R. F., Smith M. G., 1981, ARA&A, 19, 41

APPENDIX A: DERIVATION OF THE RADIATIVE TRANSFER HIERARCHY FOR ANISOTROPIC EMISSION

In this Appendix, we present a derivation of our equilibrium hierarchy, equation (29), starting from the Boltzmann equation (26) which itself was previously derived in P14. As stated in the main text, we choose a coordinate system in which the wavevector $\boldsymbol{k}$ lies along the $\hat{z}$-axis, allowing us to rewrite $\boldsymbol{n}\cdot\boldsymbol{k}$ in terms of Y_1^0; see equation (28).

To extract the spherical harmonic hierarchy, we expand all angular dependances; for any function F one has

$$F(\boldsymbol{x},\boldsymbol{n}) = \sum_{\ell',m'} F^{\ell' m'}(\boldsymbol{x}) Y_{\ell' m'}(\boldsymbol{n}), \tag{A1}$$

which is the inverse of the defining relation (7). We then multiply both sides of equation (29) by $Y^*_{\ell' m'}(\boldsymbol{n})$ and integrate over all angles $\boldsymbol{n}$. The left-hand side becomes

$$\mathrm{LHS} = \frac{ik}{a\kappa_{\mathrm{tot},0}}\sqrt{\frac{4\pi}{3}}\iint \mathrm{d}^2\boldsymbol{n} \sum_{\ell',m'} \tilde{\delta}^{\ell' m'}_{f_{\mathrm{LL}}}(\boldsymbol{k}) Y_{\ell' m'}(\boldsymbol{n}) Y_{1,0}(\boldsymbol{n}) Y^*_{\ell m}(\boldsymbol{n}) + \delta^{\ell m}_{f_{\mathrm{LL}}}(\boldsymbol{k}), \tag{A2}$$

where to obtain the last term we have applied the orthogonality relation between spherical harmonics. The first term can be simplified by applying a special case of the Wigner 3j-symbol (Varshalovich et al. 1988):

$$\iint \mathrm{d}^2\boldsymbol{n}\; Y_L^M(\boldsymbol{n}) Y_1^0(\boldsymbol{n}) Y^{*M}_{L+1}(\boldsymbol{n}) = \sqrt{\frac{3(L+M+1)(L-M+1)}{4\pi(2L+1)(2L+3)}}. \tag{A3}$$

This identity can be used to calculate the integral for two values of ℓ' in the sum given by (A2), namely $\ell' = \ell \pm 1$. The $\ell' = \ell + 1$ case is obtained by a relabelling of the indices whereas the $\ell' = \ell - 1$ case is obtained by taking the complex conjugate of equation (A3). By the triangle condition, integrals for any other value of ℓ' vanish. Consequently, we may write the LHS of our expression as

$$\mathrm{LHS} = \frac{ik}{a\,\kappa_{\mathrm{tot},0}}\left\{\sqrt{\frac{(\ell+m)(\ell-m)}{(2\ell-1)(2\ell+1)}}\tilde{\delta}^{\ell-1,m}_{f_{LL}}(\boldsymbol{k}) + \sqrt{\frac{(\ell+m+1)(\ell-m+1)}{(2\ell+1)(2\ell+3)}}\tilde{\delta}^{\ell+1,m}_{f_{LL}}(\boldsymbol{k})\right\} + \tilde{\delta}^{\ell m}_{f_{LL}}(\mathbf{k}). \tag{A4}$$

We now turn to the right-hand side of equation (29), again multiplying by $Y^*_{\ell m}(\boldsymbol{n})$ and integrating over all angles $\boldsymbol{n}$. Only $\tilde{\delta}_j$ has any angular dependence on the RHS; the orthogonality of the spherical harmonics picks out the coefficients $\tilde{\delta}_j^{\ell m}$ for this term. For all other terms, only the $\ell = 0$, $m = 0$ case survives the integration. The result is that

$$\mathrm{RHS} = (1-\beta_{\mathrm{H\,I}}\beta_r)\tilde{\delta}_j^{\ell m}(\mathbf{k}) + \frac{\delta_{\ell 0}\delta_{m0}}{\sqrt{4\pi}}\left[\beta_{\mathrm{H\,I}}\beta_r\left(\tilde{\delta}_{n_{\mathrm{H\,I}}}(\boldsymbol{k}) + \tilde{\delta}_\Gamma(\boldsymbol{k})\right) - \tilde{\delta}_{\kappa_{\mathrm{tot}}}(\boldsymbol{k})\right]. \tag{A5}$$

As expressed by equation (27), we wish to separate the radiation fluctuations that are correlated with the cosmological density field δ_ρ from those that are caused by shot noise. To do so, we need to transform some of the terms on the RHS which mix the two types of fluctuation as follows.

The terms $\tilde{\delta}_{n_{\mathrm{H\,I}}}$ and $\tilde{\delta}_\Gamma$ do not have an angular dependence and their relationships are therefore unchanged compared to P14:

$$\tilde{\delta}_{n_{\mathrm{H\,I}}} = \tilde{\delta}_{n_{\mathrm{H\,I}},u} - \tilde{\delta}_\Gamma; \quad \tilde{\delta}_{\kappa_{\mathrm{tot}}} = \beta_{\mathrm{H\,I}}\tilde{\delta}_{n_{\mathrm{H\,I}}} + \beta_{\mathrm{clump}}\tilde{\delta}_{\kappa_{\mathrm{clump}}}. \tag{A6}$$

The first of these relations arises from the fact that $n_{\mathrm{H\,I}}$ is inversely proportional to the ionization rate per H I atom, recovering the completely uniform ionizing background in the absence of any radiative fluctuations, $\tilde{\delta}_{\mathrm{n_{HI},u}}$. The effective opacity fluctuations $\delta_{\kappa_{\mathrm{tot}}}$ definition is a linear combination of the intergalactic medium absorption fluctuations and the self-shielded clump opacity fluctuations.

We can use these relations to rewrite equation (A5) in terms of $\tilde{\delta}_\Gamma$, $\tilde{\delta}_{n_{\mathrm{H\,I}},u}$ and $\tilde{\delta}_{\kappa_{\mathrm{clump}}}$. The ionization rate fluctuations $\tilde{\delta}_\Gamma$ are defined by the fluctuations in the photon density $\tilde{\delta}_{f_{\mathrm{LL}}}$ via the relation

$$\delta_\Gamma = \frac{1}{4\pi}\int \mathrm{d}^2 n\; \tilde{\delta}_{f_{LL}}(\boldsymbol{k},\boldsymbol{n}) = \frac{1}{\sqrt{4\pi}}\tilde{\delta}^{00}_{f_{\mathrm{LL}}}(\boldsymbol{k}). \tag{A7}$$

Consequently $\tilde{\delta}_\Gamma$ can be split into a correlated and shot-noise component, with $\tilde{\delta}_{\Gamma,\mathrm{SN}} \equiv \delta^{00}_{f_{\mathrm{LL}},\mathrm{SN}}/\sqrt{4\pi}$.

Using the above transformations, we find the RHS can be written

$$\mathrm{RHS} = (1-\beta_{\mathrm{H\,I}}\beta_r)\tilde{\delta}_j^{\ell m}(\boldsymbol{k}) + \beta_{\mathrm{H\,I}}\delta_{\ell 0}\delta_{m0}\tilde{\delta}^{00}_{f_{\mathrm{LL}}}(\boldsymbol{k}) + \left(\beta_{\mathrm{H\,I}}(\beta_r - 1)\,\tilde{\delta}_{n_{\mathrm{H\,I}},u}(\boldsymbol{k}) - \beta_{\mathrm{clump}}\tilde{\delta}_{\kappa_{\mathrm{clump}}}\right)\delta_{\ell 0}\delta_{m0}. \tag{A8}$$

We now apply the decomposition into cosmological and shot-noise components for $\tilde{\delta}_j$ and $\tilde{\delta}_{f_{\mathrm{LL}}}$ keeping only the shot-noise contributions. (By linearity, the two types of contribution can be treated independently and the cosmological terms are unchanged from P14.) In particular, the terms $\delta_{n_{\mathrm{H\,I}},u}$ and $\delta_{\kappa_{\mathrm{clump}}}$ are independent of radiation fluctuations; consequently they have no shot-noise component and drop out entirely. Combining equations (A4) and (A8) one reaches the final equation:

$$\begin{aligned}\tilde{\delta}^{\ell m}_{f_{\mathrm{LL}},\mathrm{SN}}(\boldsymbol{k}) - \beta_{\mathrm{H\,I}}\delta^{00}_{f_{\mathrm{LL}},\mathrm{SN}}(\boldsymbol{k})\delta_{0\ell}\delta_{0m} &+ \frac{ik}{a\,\kappa_{\mathrm{tot},0}} \times \left\{\sqrt{\frac{(\ell+m)(\ell-m)}{(2\ell-1)(2\ell+1)}}\tilde{\delta}^{\ell-1,m}_{f_{\mathrm{LL}},\mathrm{SN}}(\boldsymbol{k}) + \sqrt{\frac{(\ell+m+1)(\ell-m+1)}{(2\ell+1)(2\ell+3)}}\tilde{\delta}^{\ell+1,m}_{f_{\mathrm{LL}},\mathrm{SN}}(\boldsymbol{k})\right\} \\ &= (1-\beta_{\mathrm{H\,I}}\beta_{\mathrm{r}})\tilde{\delta}^{\ell m}_{j,\mathrm{SN}}(\boldsymbol{k}),\end{aligned} \tag{A9}$$

which agrees with the expression (29) provided in the main text.

In Section 3, we compared the solution to this hierarchy with the known isotropic limit. For these purposes, we need to extract the shot-noise-only isotropic solution in a way that was not written in P14, although it is implicit in P14 equation (38). Starting from P14's equation (30), we apply our equation (A6) and again retain only those terms which are not correlated with $\tilde{\delta}_\rho$. This yields

$$\tilde{\delta}_{\Gamma,\mathrm{SN,iso}}(\boldsymbol{k}) = \frac{(1-\beta_{\mathrm{H\,I}}\beta_{\mathrm{r}})S(k)}{1-\beta_{\mathrm{H\,I}}S(k)}\tilde{\delta}_{j,\mathrm{SN,iso}}(\boldsymbol{k}),$$

$$\text{where } S(k) = \frac{a\kappa_{\mathrm{tot},0}}{k}\arctan\frac{k}{a\kappa_{\mathrm{tot},0}}, \qquad \text{(A10)}$$

for the isotropic comparison case which is plotted as a shaded band in Fig. 2.

This paper has been typeset from a TEX/LATEX file prepared by the author.